JOURNAL OF CATALYSIS 70, 335–346 (1981)

Physical Characterization of Fe/TiO_2 Model Supported Catalysts

III. Combined Electron Microscopic and Spectroscopic Studies of Reduction and Oxidation Behavior

B. J. TATARCHUK[1] AND J. A. DUMESIC[2]

Department of Chemical Engineering, University of Wisconsin, Madison, Wisconsin 53706

Received December 2, 1980; revised April 3, 1981

The combination of results from transmission electron microscopy, X-ray photoelectron spectroscopy, and conversion electron Mössbauer spectroscopy are used to summarize and discuss the behavior of Fe/TiO_2 model supported catalytic specimens following hydrogen and oxygen treatments at progressively higher temperatures. During hydrogen treatment, initial iron overlayers (ca. 5 nm thick) on TiO_2 undergo reduction, nucleation, and growth to small metallic iron particles at temperatures from 608 to 707 K; these iron crystallites spread over (or wet) the titania support at 773 K, forming particles with a "thin-crystal" morphology; and at 875 K, iron facilitates reduction of titania, accompanied by the diffusion of iron into the support. Following this high-temperature reduction, samples were treated in oxygen at ca. 950 K. Some of the iron that had diffused into the support returned to the surface. This high-temperature oxidation does not, however, simply reverse the effect of high-temperature reduction. Instead, the iron is converted into large particles of $FeTi_2O_5$. The lack of reversibility during sequential hydrogen and oxygen treatments at high temperatures is attributed to strong interactions between iron and titanium, manifested by the formation of dispersed and strongly interacting iron (e.g., γ-Fe; Fe_xTi, $1 \leq x \leq 2$) or $FeTi_2O_5$ under reducing or oxidizing conditions, respectively.

INTRODUCTION

The previous two parts of this series dealt with electron microscopic (Part I) and electron spectroscopic (Part II) investigations of Fe/TiO_2 model supported catalysts. In short, titania films covered with iron overlayers of either 5 nm or 3.8 nm were heated in hydrogen to progressively higher reduction temperatures, and various phenomena were thereby noted and studied. In particular, these phenomena included nucleation of the iron overlayer into iron particles, reduction of the iron to the metallic state, spreading (or wetting) of iron over the support, reduction of Ti^{4+} to lower valence states, and diffusion of iron into the support. Table 1 shows a summary of these results for the 5-nm iron overlayer. Yet, it is through a combination of different techniques that better understanding of the various phenomena can be achieved. Thus, while the first two parts of this series involved a technique-oriented discussion of the Fe/TiO_2 system, the present paper is a phenomenon-oriented discussion of this metal–support system. Accordingly, the two preceding papers discussed the different columns of Table 1 while the present paper considers the various rows.

Another aspect of the Fe/TiO_2 system is its response to oxidation treatments. Indeed, it has been found by others (*1–4*) that the strong interactions between titania and various supported Group VIII metals can be destroyed by high-temperature (ca. 770 K) oxygen treatment. Thus, oxidation studies of Fe/TiO_2 may provide information complementary to that obtained by the previous reduction studies (Parts I and II). For this reason the present paper also

[1] Present address: Department of Chemical Engineering, Auburn University, Auburn, Alabama 36849.

[2] To whom correspondence should be addressed; Camille and Henry Dreyfus Foundation Teacher-Scholar.

0021-9517/81/080335-12$02.00/0

TABLE 1

TEM, XPS, CEMS Reduction Summary (5.0 nm Fe)

Reduction temperature (K)	Observed TEM trends	Observed XPS trends	Observed CEMS trends	Reduction regimes
Initial iron overlayer	Contiguous Fe film	Fe^{3+}/Ti^{4+}	55% Fe^{2+}, 32% Fe^0, 13% Fe^{3+}	Low-temperature reduction, nucleation, and growth
608	Nonuniform nucleation, most probable particle size,	Fe^0 and Fe^{2+}/Ti^{4+}	59% Fe^{2+}, 41% Fe^0	
643	$\langle D \rangle < 10$ nm	Fe^0/Ti^{4+}	57% Fe^0, 43% Fe^{2+}	
677	Uniform nucleation; three-dimensional crystallites,	Fe^0/Ti^{4+}	100% Fe^0	
707	$\langle D \rangle > 10$ nm			
773	Contrast between crystallites, $\langle D \rangle \cong 10$ nm	Fe^0/Ti^{4+}	Fe^0, broadened spectrum	Spreading of iron over support
875	Contrast between crystallites, decrease in number, density, and volume of crystallites,	Decrease in Fe spectral area, increase in Ti spectral area, reduction of Ti^{4+}	Spectral singlet (e.g., γ-Fe, Fe_xTi), ~32% decrease in spectral area	Diffusion of iron into support
973	$\langle D \rangle \leq 10$ nm			

presents and discusses transmission electron microscopy (TEM), X-ray photoelectron spectroscopy (XPS), and conversion electron Mössbauer spectroscopy (CEMS) studies designed to monitor the morphological and chemical changes in the Fe/TiO_2 system that result from high-temperature oxidation.

EXPERIMENTAL

The samples used in the oxidation studies were those specimens which had been previously reduced during the reduction studies in Parts I and II of this series. In short, they were derived from 5.0-nm or 3.8-nm iron overlayers on TiO_2 films, as described in Part I.

The equipment and procedures employed in these TEM, XPS, and CEMS studies are the same as those described earlier. In particular, the TEM methodology was presented in Part I while the experimental aspects of XPS and CEMS were presented in Part II.

RESULTS

Reduction

The results of the reduction studies of Parts I and II are summarized in Table 1.

Oxidation

The samples used for the reduction studies of Parts I and II were subsequently oxidized and in some cases re-reduced as shown in Table 2. TEM, XPS, and CEMS were then used to monitor the accompanying morphological and chemical changes.

Figure 1 shows the transmission electron micrographs from both the 5.0-nm and 3.8-nm specimens following oxidation at 918 K. Included also are the corresponding particle size distributions and particle volume

TABLE 2

Sample Treatment Conditions

TEM[a] (Temperature/Time)	XPS[a] (Temperature/Time)	CEMS[b] (Temperature/Time)
	Oxidation[c]	
918 K/3.0 h	943 and 973 K/3.0 h	674 K/1.0 h
		777 K/1.0 h
		876 K/1.0 h
		922 K/3.0 h
		979 K/2.0 h
	Re-reduction[d]	
—	958 K/3.0 h	—

[a] Oxidation in O_2 at 1.33×10^{-2} Pa.

[b] Oxidation in O_2 at 1.33×10^{-3} Pa.

[c] Oxidation and re-reduction treatments shown here have been performed on samples previously reduced as described in Table 1, Part I.

[d] Reduction at $P_{H_2}/P_{H_2O} \cong 100$; total pressure $\cong 1.33 \times 10^{-2}$ Pa.

distributions tabulated after counting approximately 600 particles per distribution. By comparison, the corresponding electron micrographs and particle size distributions taken for the 5-nm iron sample prior to high-temperature oxidation were presented in Part I (Figs. 3 to 8). It can be seen that a significant growth of the iron particles has taken place during this oxidation treatment. The 3.8-nm iron sample behaves in a similar manner.

X-Ray photoelectron spectra taken after high-temperature oxidation revealed that all of the titanium was converted to Ti^{4+}, and all of the iron was present as Fe^{3+}. This was determined by measuring the positions of the Fe-$2p_{3/2}$ peak and the Ti-$2p_{3/2}/2p_{1/2}$ doublet, as shown by the broken spectra in Figs. 3 to 5 of Part II. At the same time, the Ti/Fe spectral area ratio was observed to decrease, shown by the broken portion of Fig. 6 in Part II, to a value of ca. 30 for the 5-nm iron sample. Following this oxidation treatment, the 5-nm iron sample was re-reduced at 958 K in hydrogen, and it can be seen in Fig. 6 (Part II) that the Ti/Fe area ratio increased once again, to a value of ca. 100.

Following this re-reduction of the 5.0-nm iron sample, Ar sputtering was employed to probe the iron concentration at various depths into the surface. In particular, the Fe/Ti spectral area ratio was measured after various exposure times to a d.c. Ar beam (2 kV, 25 $\mu A/cm^2$); the spectral area ratio was then converted into an atomic ratio using the appropriate photoelectric cross sections and instrumental sensitivity factors (*5*, *6*), while sputtering times were converted into approximate depths by measuring the sputter rates of targets of known thickness and with similar sputter yields. The corresponding Fe/Ti depth profile for the re-reduced 5-nm iron sample is shown in Fig. 2. For comparison, Fig. 2 also shows the Fe/Ti depth profile for the 3.8-nm iron sample following oxidation at 943 K. It should be noted that the maximum in the plot of the Fe/Ti ratio versus depth occurs closer to the surface for the oxidized 3.8-nm iron sample than for the re-reduced 5.0-nm iron sample.

Figure 3 contains the room-temperature conversion electron Mössbauer spectra following oxygen treatment, at progressively higher temperatures, of the previously reduced 5-nm iron sample (see Fig. 7 of Part II). Oxygen treatment at 674 K has little

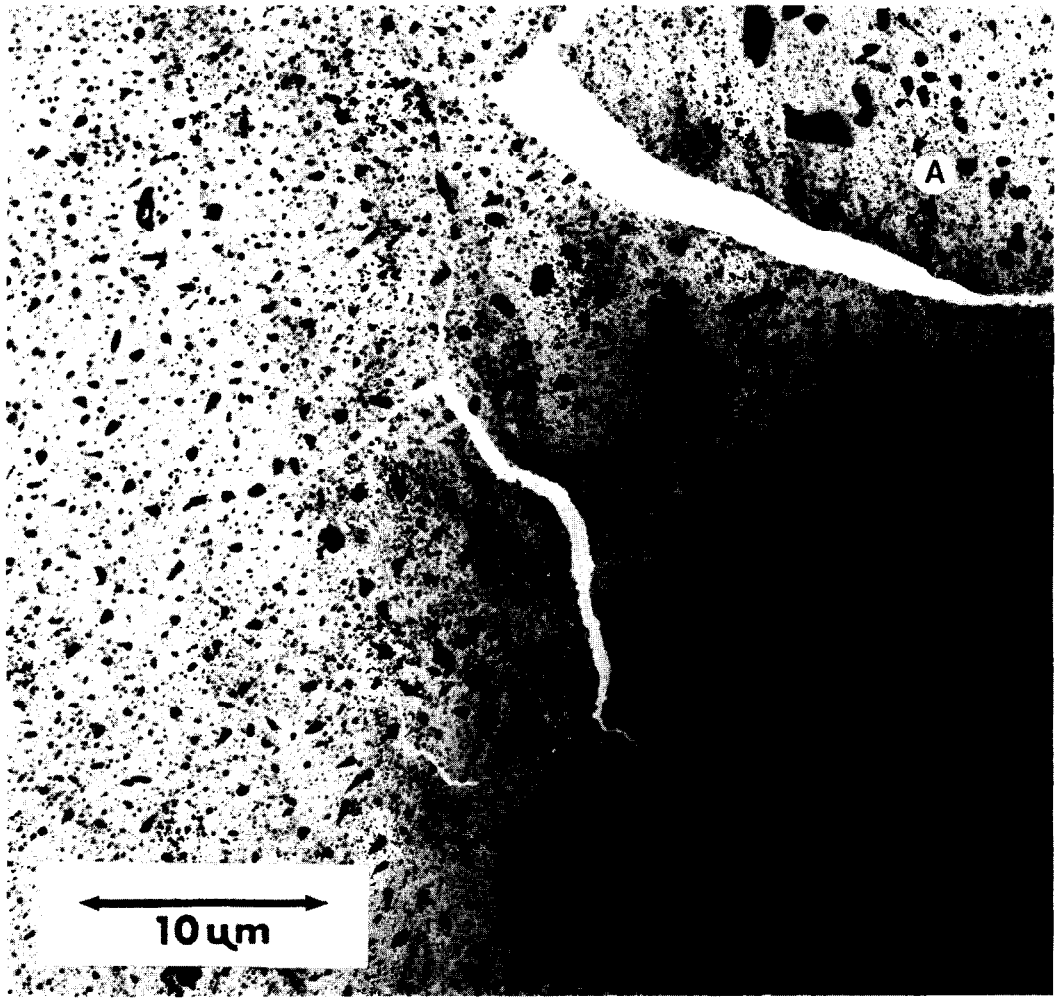

FIG. 1. Transmission electron micrographs and particle size/volume distributions for 5.0-nm and 3.8-nm Fe/TiO_2 samples following oxidation at 918 K (Table 2) of previously reduced specimens (Table 1, Part I). (A,B,C): 5-nm iron sample; (D,E,F): 3.8-nm iron sample.

effect on the Mössbauer spectrum, while treatment at higher temperatures (up to 979 K) leads primarily to the formation of a new spectral doublet centered at 1.05 mm/s (with respect to metallic iron) with a quadrupole splitting of 2.2 mm/s. Accompanying the formation of this doublet there is also a 55% decrease in the spectral area. A small amount of the α-Fe_2O_3 sextuplet (the peak positions of which are indicated by the lines at the top of the figure) is also detectable in the spectrum recorded after oxidation at 876 K.

DISCUSSION/SUMMARY

Reduction Behavior

It was noted in Part II of this series that the reduction behavior of Fe/TiO_2 samples may be divided into three regimes. These are summarized in Table 1 for the 5-nm iron sample. Consider first the different phenomena that take place in Regime I during reduction at progressively higher reduction temperatures up to 707 K. TEM (*7*) analysis of the initial iron overlayer showed the presence of a contiguous iron film. XPS

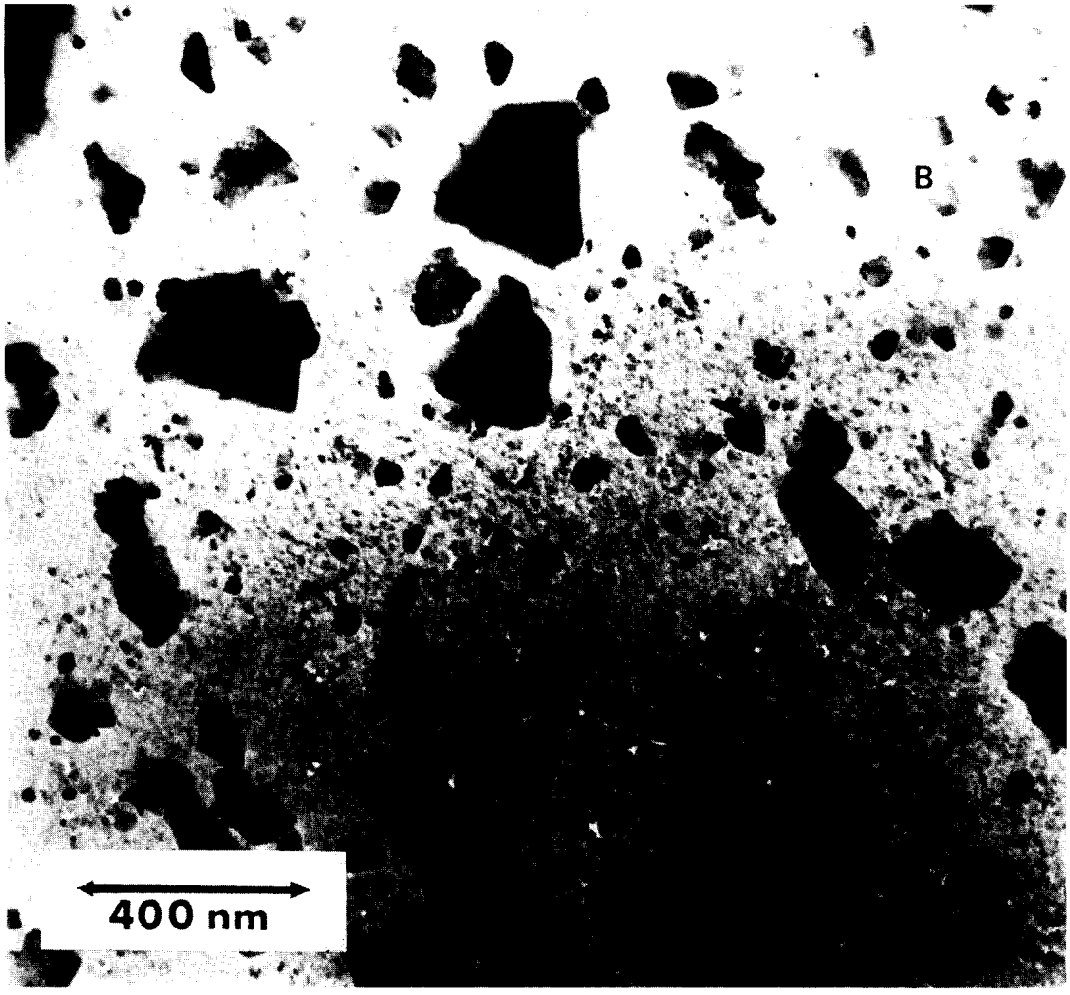

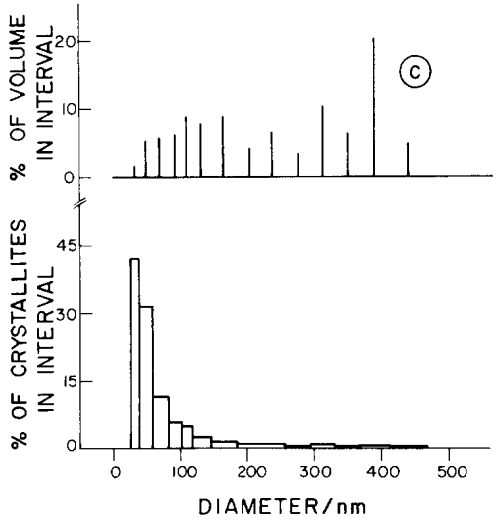

FIG. 1—*Continued.*

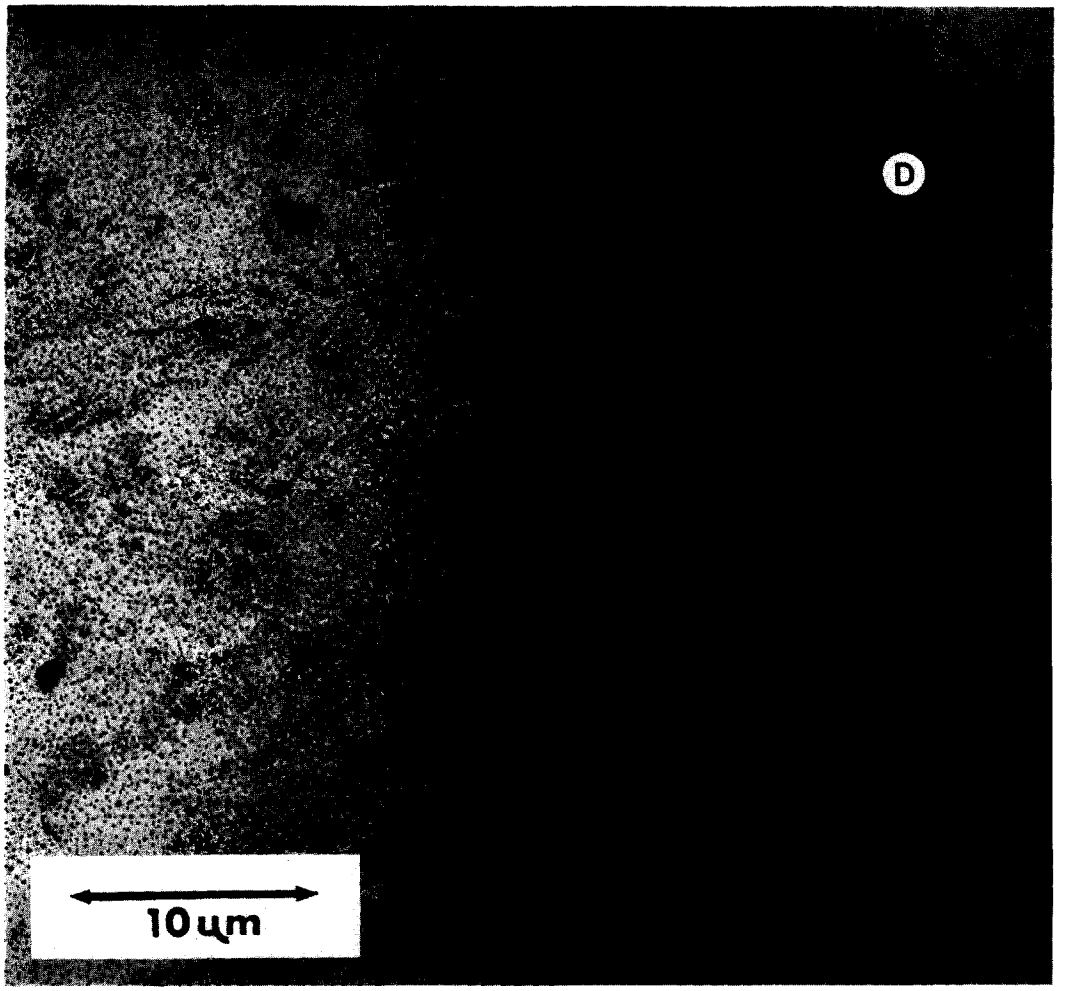

FIG. 1—*Continued*

measurements (*8*) agreed with this conclusion by virtue of a small absolute Ti/Fe concentration ratio. It was also observed that essentially all of the iron detectable by XPS was present as Fe^{3+}. CEMS (*8*), however, revealed in addition to Fe^{3+}, the existence of metallic iron and Fe^{2+} in the iron overlayer. These differences are due to the greater sampling depth for CEMS compared to XPS. Thus, since CEMS probes essentially all of the iron overlayer while XPS monitors only the top 2 nm, it is concluded that the Fe^{3+} lies on the surface of the overlayer.

Reduction through the first two temperatures (608 and 643 K) resulted in a partial nucleation of the iron overlayer on various regions of the TiO_2 film, as observed by TEM. XPS results for the 5-nm iron sample indicated essentially complete conversion of iron to Fe^0 following reduction at 608 K. For the 3.8-nm iron sample, however, XPS measurements showed the continued presence of a Fe^{2+} component after treatment at 608 K. These XPS results indicate that while the topmost ~2.0 nm of the external iron surface (film and/or particles) is metallic, the iron lying below this surface (e.g., adjacent to the support) is in the Fe^{2+} state. This is shown schematically in Fig. 4A. CEMS supports this interpretation by verifying the presence of Fe^{2+} in the 5-nm

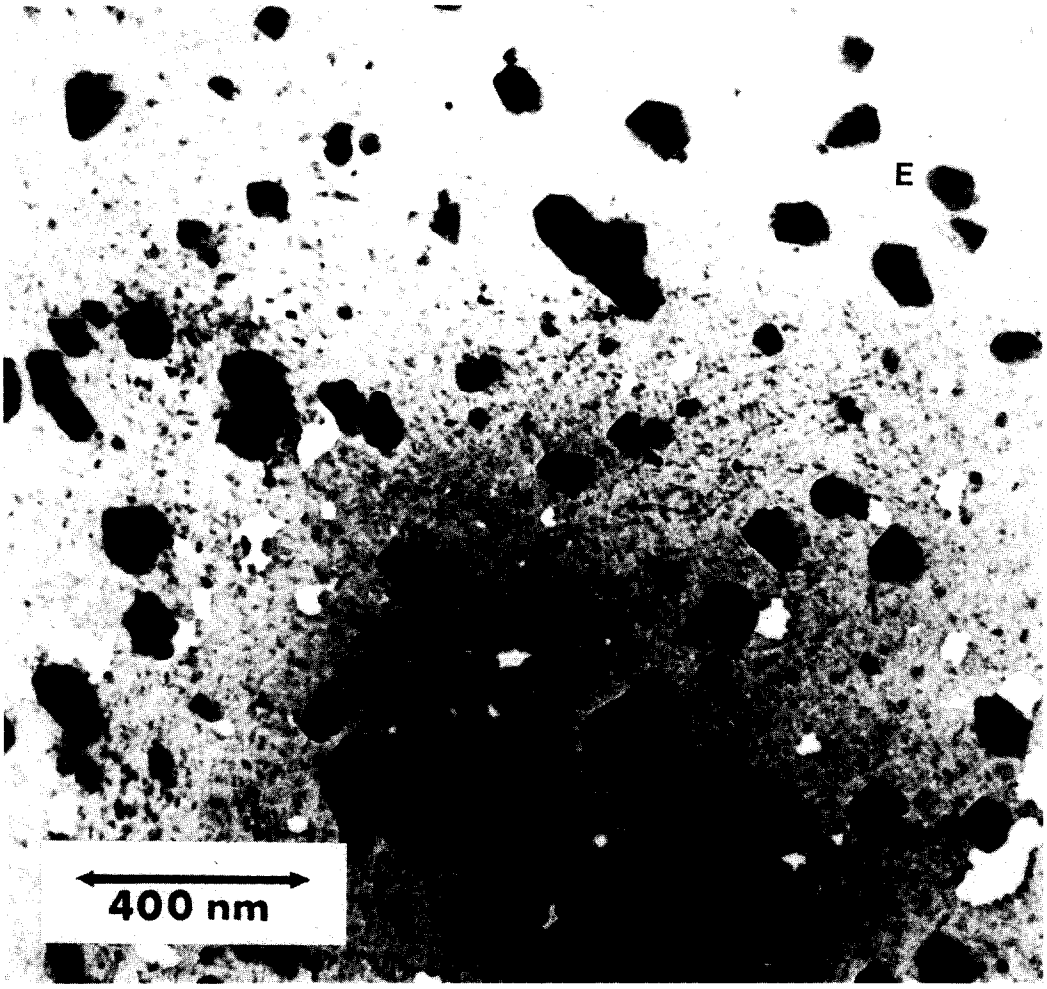

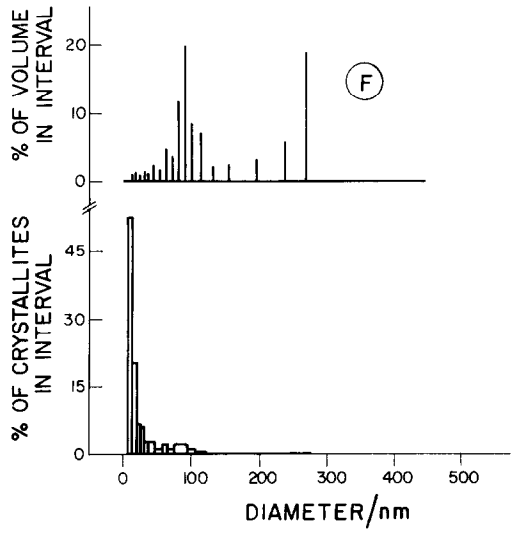

FIG. 1—*Continued*

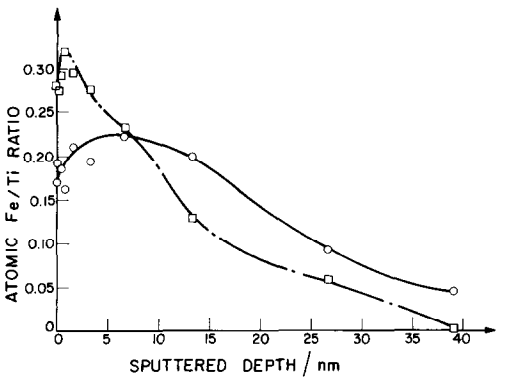

FIG. 2. Fe/Ti atomic ratio determined by XPS versus sputtered depth: (□) 3.8-nm Fe/TiO_2 sample following oxidation at 943 K (Table 2) of a specimen previously reduced at 963 K (Table 1, Part I); (○) 5.0-nm Fe/TiO_2 sample following re-reduction at 958 K (Table 2) of a specimen first reduced at 973 K (Table 1, Part I) and subsequently oxidized at 973 K (Table 2).

overlayer after treatment at 608 K, when XPS detected only Fe^0.

Reduction at 677 K resulted in uniform nucleation of iron over the entire titania surface. This corresponds to the complete reduction of iron to the metallic state, as measured by both XPS and CEMS (see Fig. 4B). At this temperature, the metallic iron particles were present as three-dimensional crystallites (as evidenced by TEM) on a fully oxidized TiO_2 support (as determined by XPS). Heating to 707 K led to some sintering of the metallic iron particles, but the three-dimensional character of these particles was preserved.

Regime II is entered upon reduction at 773 K, at which temperature the iron particles spread over (or wet) the titania support. In particular, after this treatment the smaller iron particles were transformed into thin metallic crystallites which showed a low contrast (TEM) with respect to the titania support. This is shown schematically in Fig. 4C. It has been proposed previously that such wetting behavior may be accompanied by (or related to) partial reduction of the support. In the present study no reduction at 773 K was observed using XPS; however, if this reduction is confined to local regions of the support near (or below) the iron crystallites, it is possible that it would not be readily detectable via these XPS measurements. Further evidence for the spreading of iron over the support in Regime II is that the metallic iron particle size distribution (from TEM) adopted a slightly bimodal shape and the Mössbauer spectral peaks broadened significantly following hydrogen treatment at 773 K.

Reduction at 875 K leads to the phenomena of Regime III. XPS measurements indicated that Ti^{4+}, in iron-containing samples, is reduced to lower valence states during this treatment. In contrast, iron-free samples did not show this reduction of Ti^{4+}, indicating that iron facilitates reduction of the support. TEM analyses after this treatment again showed the presence of the "thin-crystal" morphology, with this particle morphology extended to crystallites of larger diameter compared to the behavior of Regime II. Comparison of particle size

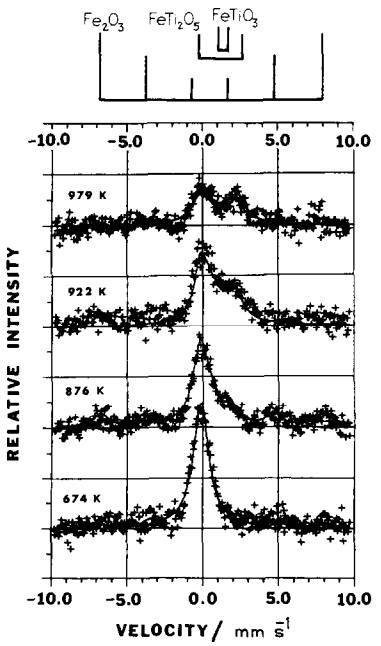

FIG. 3. Conversion electron Mössbauer spectra of 5.0-nm Fe/TiO_2 sample following reduction at temperatures through 875 K (Table 1, Part I) and oxidation at the indicated temperatures (Table 2). One vertical square is equivalent to 2% effect.

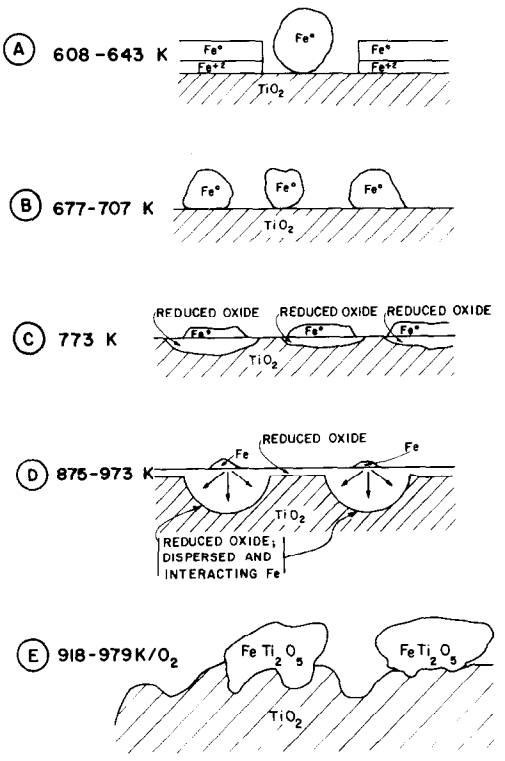

FIG. 4. Schematic diagram of the Fe/TiO_2 system after reduction at progressively higher temperatures followed by oxidation.

distributions indicated a shift toward smaller particles upon treatment in Regime III (i.e., apparent redispersion) and TEM contrast calculations (mass balances) demonstrated that this change in shape of the particle size distributions cannot be explained by atomistic sintering on the surface of the support. In fact, by monitoring the size and number of crystallites per unit area of support, it was shown that, within the resolution of the TEM (1.5 nm), the amount of highly contrasted material present as distinct particles decreased by approximately 50% between the treatment temperatures of 707 and 973 K. This then indicates that at least one source of this apparent redispersion may be the loss of highly contrasted material. XPS measurements were consistent with the loss of surface iron as the intensity of the iron $2p_{3/2}$ signal decreased markedly following this high-temperature treatment. CEMS also showed a 30% decrease in spectral area, attributed to the electron attenuation which occurs from iron atoms located far below the surface. The results from TEM, XPS, and CEMS thus reveal that iron diffuses into the titania at temperatures of 875 K or higher. XPS also shows the presence of reduced titanium species following this hydrogen treatment. Indeed, the diffusion of iron into the support and the reduction of titania may well be interrelated Specifically, iron facilitates the reduction of titania, and the removal of oxygen from titania during this reduction allows iron to diffuse into the support. This is shown schematically in Fig. 4D. During this process, the iron is converted into a dispersed and strongly interacting state within the support. Specifically, CEMS shows the presence of a spectral singlet consistent with the formation of γ-Fe or Fe_xTi ($1 \leq x \leq 2$). The existence of either of these phases requires a strong interaction with the support: the γ-Fe structure (fcc) formed by growth within a support matrix (*9, 10*), and Fe_xTi formed by incorporation of Ti into Fe.

After treatment at 963 K or higher temperatures, the presence of reduced titanium species was observed by XPS on titania films that did not contain iron. The origin of this reduction is not well understood. For example, it may be partially due to the presence of carbon at the surface (observed in Part II by XPS) and/or a restructuring of the TiO_2 film (observed in Part I by TEM: Fig. 2B). While XPS did not detect any change in the carbon concentration at the surface upon hydrogen treatment at 963 K, it is known that impurities such as carbon can facilitate the reduction of titania (*11–13*).

Oxidation Behavior

It was shown by XPS that oxidation at 943 or 973 K of samples previously reduced at 963 and 973 K leads to a partial restora-

tion in the surface iron concentration (see Figs. 3, 4, and 6 of Part II). In addition, Fig. 5 of Part II clearly indicates that the titanium is returned to the Ti^{4+} state while Figs. 3 and 4 (Part II) show that the iron is oxidized to Fe^{3+} following this treatment.

Complementary to these findings are the results of CEMS. It is seen in Fig. 3 that the singlet peak indicative of a strong interaction during reduction is oxidized only at temperatures greater than 674 K. This is consistent with the previous results indicating that iron has diffused into the support following the initial high-temperature reduction. After oxidation at 876 K a shoulder can be observed on the positive-velocity side of the strongly interacting singlet peak. The position of this shoulder is consistent with the presence of ilmenite ($FeTiO_3$). In addition, oxidation at this temperature leads to an increase in the intensity of the spectral sextuplet due to α-Fe_2O_3. Finally, the ultimate oxidation product after treatment at 979 K is Fe^{2+}, as determined by the isomer shift of the resulting spectral doublet. Furthermore, the Mössbauer parameters of this doublet suggest that the Fe^{2+} is present in the form of the pseudobrookite-like compound $FeTi_2O_5$ (*14, 15*). It is not known to what extent the ilmenite and α-Fe_2O_3, observed at lower temperatures, are intermediates in the eventual formation of $FeTi_2O_5$. Previous investigators (*14, 15*) have, in fact, produced $FeTi_2O_5$ by reaction between α-Fe_2O_3 and TiO_2, with trace amounts of ilmenite observed (*15*) as expected from thermodynamic consideration (*16*). Of importance is the fact that $Fe^{2+}Ti_2O_5$ and $Fe_2^{3+}TiO_5$ can form a solid solution under these conditions, yet the observed Fe^{2+} species (CEMS) is somewhat expected in view of the excess Ti present. It is clear, however, that the interactions between Fe and TiO_2 cannot be destroyed by high-temperature oxidation. Specifically, iron–titanium mixed oxides are formed.

Comparison of XPS and CEMS results further indicates that the mixed oxides formed upon high-temperature oxidation must be poorly dispersed. This follows in order that the "surface" iron is Fe^{3+} (as shown by XPS) while the "bulk" iron is Fe^{2+} (as shown by CEMS). This conclusion is supported by the 55% decrease in total Mössbauer spectral area accompanying the oxidation of the strongly interacting singlet peak to $FeTi_2O_5$ (see Fig. 3). That is, a large fraction of the total crystallite volume must be located in sufficiently large particles of $FeTi_2O_5$ (see Figs. 1C and F) so that attenuation of the conversion and Auger electrons occurs from iron atoms deep within these particles.

TEM studies of the 5-nm and 3.8-nm iron samples *after high-temperature oxidation* confirm the growth of large crystallites (see Figs. 1A through F). This is shown by comparing the electron micrographs and the particle size distribution for the 5-nm iron sample following oxidation (Figs. 1A through C) with the results of Part I which show the iron particles of this same sample *prior* to oxidation but following reduction (Figs. 3–8 of Part I). The two low-magnification micrographs of the oxidized 3.8-nm and 5.0-nm iron samples (Figs. 1A and D) also indicate that the crystallites observed following oxidation are indeed related to iron, as the volume of highly contrasted material (assuming three-dimensional particles) is proportional to the initial iron overlayer thicknesses. The contrast balances performed on TEM specimens reduced at 707 K, assuming cubic particle geometry as described in Part I, were then compared to those performed on micrographs taken following oxidation of these same specimens at 918 K. In short, these calculations involve use of the particle volume distribution and knowledge of the number of particles per unit area of the titania surface to determine the volume of iron-containing phases present on the support as discrete particles. The results of these measurements indicate that there is an increase in the volume of iron-containing material, following oxidation, by factors of

8.2 and 7.3 for the 5.0- and the 3.8-nm iron specimens, respectively. This increase in total crystallite volume can be attributed to the formation of an iron–titanium mixed oxide phase. Making use of the known densities of Fe^{2+}–Ti^{4+} mixed oxides, it is possible to calculate the expected volume increases that would result if 1 cm^3 of metallic iron were converted into the corresponding volume of mixed oxide. Indeed, it is found that the expected volume increase for formation of the ferrous pseudobrookite phase ($FeTi_2O_5$) is 7.48, while that for ilmenite ($FeTiO_3$) is only 4.53. While other Ti^{4+}/Fe^{2+} mixed oxides do in fact exist (e.g., $Fe_{3-x}Ti_xO_4$, etc.) (*17*), these calculations are nevertheless consistent with the formation of $FeTi_2O_5$ suggested by CEMS.

The previously noted increase in the surface iron concentration upon high-temperature oxidation (as shown in the broken portions of Figs. 3, 4, and 6 in Part II) indicates that many of the $FeTi_2O_5$ crystallites are located on the surface of the TiO_2 film. This is shown schematically in Fig. 4E. In contrast, the iron is present within the titania film following high-temperature reduction. The results of Ar sputter profiling for Fe and Ti support these conclusions that iron diffuses into the support during high-temperature reduction while iron is partially returned to the surface (in the form of large $FeTi_2O_5$ particles) following high-temperature oxidation of a previously reduced specimen. Indeed, the plots of the XPS-Fe/Ti atomic ratio versus depth into the sample (see Fig. 2) show that the maximum iron concentration is located closer to the surface of an oxidized sample than for a reduced sample. Unfortunately, a number of complications exist which prevent the direct quantitative interpretation of these profiles (*18*). The most serious of these complications is the fact that these samples consist of discrete iron-containing particles (of different composition and sputter yield) on a titania film. Sputter profiles thus reflect the removal of material from both the iron-containing particles and the support itself. Large particles on the support would give the appearance of iron present at great depths into the support while small particles on the support would give the appearance of iron present near the surface of the support. The average iron particle size is much larger for the oxidized samples, however, and this effect cannot explain the observed differences in sputter profiles for the oxidized and reduced samples.

Re-reduction at 958 K of these oxidized samples (see Table 2) results in a decrease in the surface iron concentration as indicated by Fig. 2 and the broken portions of Figs. 3 and 6 in Part II. The surface iron concentration does not, however, return to that value observed following the first high-temperature reduction, indicating that the movement of iron to and from the surface in oxygen and hydrogen respectively is not completely reversible. Furthermore, as discussed in Part II, this change in iron concentration cannot be explained by the removal of carbon and/or oxygen from the surface during reduction of the support. This lack of reversibility is not unexpected, as the iron is present in Ti-free phases prior to the first reduction (e.g., as iron oxides and metallic iron), while it is present in an Fe–Ti mixed oxide phase prior to the re-reduction. In addition, the first high-temperature reduction involves small iron particles formed during reduction and nucleation of the initial iron overlayer, while the high-temperature re-reduction involves large iron-containing particles of poorly dispersed $FeTi_2O_5$. Thus, the lack of reversibility during sequential hydrogen and oxygen treatments at high temperatures is attributed to strong Fe–Ti interactions: formation of dispersed and strongly interacting iron (e.g., γ-Fe, Fe_xTi) upon reduction and formation of $FeTi_2O_5$ upon oxidation.

ACKNOWLEDGMENTS

Financial support for this research (Parts I through III of this series) was received from the National

Science Foundation (Grant ENG77-08481) and is gratefully acknowledged. One of us (B.J.T.) also wishes to thank Chevron for providing a graduate fellowship during a portion of this work. The assistance of B. Clausen in adaptation of the Mössbauer fitting routine for use in CEMS is also appreciated. Finally, we wish to express our gratitude to S. J. Tauster and R. T. K. Baker (at Exxon) for their insightful discussions and also to R. L. Garten for helpful comments during the early stages of this research.

REFERENCES

1. Tauster, S. J., Fung, S. C., and Garten, R. L., *J. Amer. Chem. Soc.* **100,** 170 (1978).
2. Baker, R. T. K., Prestridge, E. B., and Garten, R. L., *J. Catal.* **56,** 390 (1979).
3. Meriaudeau, P., Ellestad, H., and Naccache, C., *in* "Proceedings, 7th International Congress on Catalysis, Tokyo, 1980," Paper No. E2.
4. Gajardo, P., Gleason, E. F., Katzer, J. R., and Sleight, A. W., *in* "Proceedings, 7th International Congress on Catalysis, Tokyo, 1980," Paper No. E1.
5. Scofield, J. H., *J. Electron Spectrosc. Relat. Phenom.* **8,** 129 (1976).
6. Wagner, C. D., Riggs, W. M., Davis, L. E., and Moulder, J. F., *in* "Handbook of X-Ray Photoelectron Spectroscopy" (G. E. Muilenberg, Ed.), Perkin–Elmer Corporation, 1979.
7. Tatarchuk, B. J., and Dumesic, J. A., *J. Catal.* **70,** 308 (1981).
8. Tatarchuk, B. J., and Dumesic, J. A., *J. Catal.* **70,** 323 (1981).
9. Gonser, U., Meechan, C. J., Muir, A. H., and Wiedersich, H., *J. Appl. Phys.* **34,** 2373 (1963).
10. Gonser, U., Grant, R. W., Meechan, J., Muir, A. H., and Wiedersich, H., *J. Appl. Phys.* **36,** 2124 (1965).
11. Iyengar, R. D., and Codell, M., *Advan. Colloid Interface Sci.* **3,** 365 (1972).
12. Gebhardt, J., and Herrington, K., *J. Phys. Chem.* **62,** 120 (1958).
13. Iyengar, R. D., and Kellerman, R., *Z. Phys. Chem. (Frankfurt am Main)* **64,** 345 (1969).
14. Shirane, G., Cox, D. E., and Ruby, S. L., *Phys. Rev.* **125,** 1158 (1962).
15. Grey, I. E., and Ward, J., *J. Solid State Chem.* **7,** 300 (1973).
16. Grey, I. E., Reid, A. F., and Jones D. G., *Inst. Mining Met.* **83,** C105 (1974).
17. Umemura, S., and Iida, S., *J. Phys. Soc. Japan* **44,** 341 (1978).
18. Wehner, G. K., Chapter 1 in "Methods of Surface Analysis" (A. W. Czanderna, Ed.), Elsevier, New York, 1975.